Research Square

Preprints are preliminary reports that have not undergone peer review.
They should not be considered conclusive, used to inform clinical practice,
or referenced by the media as validated information.

Microporous Polymer Adsorptive Membranes with Unprecedented Processing Capacity for Molecular Separation

Zhenggong Wang
Soochow University
Xiaofan Luo
Soochow University
Kuan Lu
Institute of Coal Chemistry, Chinese Academy of Sciences
Shouwen Zhu
Soochow University
Yanshao Yang
Suzhou Institute of Nano-Tech and Nano-Bionics, Chinese Academy of Sciences
Zejun Song
Suzhou Institute of Nano-Tech and Nano-Bionics, Chinese Academy of Sciences
Wangxi Fang
Suzhou Institute of Nano-tech and Nano-bionics
Yatao Zhang
Zhengzhou University https://orcid.org/0000-0002-6832-3127
Jian Jin (jjin@suda.edu.cn)
Soochow University

Article

Keywords:

Posted Date: December 10th, 2021

DOI: https://doi.org/10.21203/rs.3.rs-1132837/v1

License: This work is licensed under a Creative Commons Attribution 4.0 International License.
Read Full License

Version of Record: A version of this preprint was published at Nature Communications on July 19th, 2022. See the published version at https://doi.org/10.1038/s41467-022-31575-y.

Abstract

Trade-off between permeability and nanometer-level selectivity is an inherent shortcoming of membrane-based separation of molecules, while most highly porous materials with high adsorption capacity lack solution processability and stability for achieving adsorption-based molecule separation. We hereby report a hydrophilic amidoxime modified polymer of intrinsic microporosity (AOPIM-1) as a membrane adsorption material to selectively adsorb and separate small organic molecules from water with ultrahigh processing capacity. The membrane adsorption capacity for Rhodamine B reaches 26.114 g m^{-2}, 10~1000 times higher than previously reported adsorptive membranes. Meanwhile, the membrane achieves >99.9% removal of various nano-sized organic molecules with water flux 2 orders of magnitude higher than typical pressure-driven membranes of similar rejections. This work confirms the feasibility of microporous polymers for membrane adsorption with unprecedented capacity, and provides the possibility of adsorptive membranes for molecular separation.

Introduction

Molecular separation is an essential component in many human daily activities and multiple industrial, medical, and environmental processes, such as water purification, oil and gas refining, energy generation and storage, pharmaceutical ingredient extraction and purification[1–5]. Among various materials and methods, synthetic membranes and membrane-based separation have been extensively studied due to its strong sustainability, scale-up feasibility, and no phase change during separation[1,6]. However, trade-off between membrane permeability and selectivity is an inherent shortcoming of membrane-based molecular separation[7–8]. Taking pressure-driven membrane processes for instance, microfiltration and ultrafiltration membranes exhibit high water permeation flux and reject large molecules with high efficiency, but their large pores (0.002-1 μm) are unable to separate nanometer-sized small organic molecules[9]. Processing of these small organic molecules requires membranes of nanofiltration level pore size and selectivity, yet the reduction in pore size inevitably results in much lower water permeation flux[10]. In contrast, adsorption can be a highly selective molecular separation process with specific physical or chemical interactions between adsorbents and target molecules[11–14], but its application is often limited by its low processing rate, high internal diffusion resistance within absorbents, etc[15–16]. Membrane adsorption is a pressure-driven dynamic membrane-based adsorption process, which combines the merit of both adsorption and membrane separation[17–19]. Compared to traditional pressure-driven membranes with size sieving as the dominant separation mechanism, adsorptive membranes utilize more specific membrane-solute interactions like electrostatic interactions, π-π interactions, van der Waals forces, and hydrogen bonding to achieve highly selective and fast separation of small organic molecules[20–21]. Therefore, they are expected to break through the permeability-selectivity trade-off by simultaneously achieving the selectivity of dense membranes and permeability of porous membranes[18,22–25].

However, the application of membrane adsorption is hindered by the lack of adsorptive membranes with sufficient processing capacity. Adsorptive membranes are usually prepared by post-grafting affinity

ligands or adsorptive filler mixing in traditional polymer materials[15,20]. Due to the limited specific surface area and adsorption sites incorporated, the overall processing capacity of these conventional adsorptive membranes is very low, mostly in the range of 0.01-1 g m^{-2}. Such membranes could only handle solutions of very low concentration and require frequent cleaning and regeneration, which greatly affects their further development and practical application. Although porous materials such as metal-organic frameworks (MOFs) possess large porosities and rich affinity sites[18–19, 26–30], their poor solution processability hinders their engagement as absorptive membrane separation materials. Besides, most MOFs materials do not have sufficient stability in water, especially under acidic or alkaline conditions, resulting in membrane failure during long-term operation[8].

In this work, we report a microporous polymer based adsorptive separation membrane, which has extremely high adsorption capacity and can realize fast and selective molecular separation. The microporous polymer is amidoxime modified polymer of intrinsic microporosity (AOPIM-1) polymer, which owns a rigid and contorted three-dimensional structure in its backbone. The ineffective chain packing brings high specific surface area up to 550 m^2 g^{-1} and produces interconnected free volumes with a size of less than 2 nm[31–34]. The amidoxime modification endows the polymer with good solution processability and provides abundant adsorption sites for selectively adsorbing charged molecules. Due to its unique chemical and physical structure, it achieves a high-efficiency removal of small organic molecules (>99.9%) with permeating flux 2 orders of magnitude higher than typical nanofiltration membranes of similar dye rejections, and such separation performance is maintained throughout multiple adsorption-elution cycles with >98% flux recovery rate (FRR). More importantly, the static adsorption capacity of the membrane material greatly surpasses traditional non-porous polymer adsorbents and comparable to MOF-based adsorbents, while the dynamic processing capacity reaches 26.114 g m^{-2}, much higher than all the adsorptive membranes reported so far. The unprecedented processing capacity is expected to enable the membrane towards more realistic adsorption-separation application scenarios.

Results And Discussion

Material characterization of AOPIM-1 polymer

Polymer of intrinsic microporosity (PIM-1) was synthesized via a polycondensation reaction between TTSBI and TFTPN (Figure S1) as reported previously[35], which shows a high specific surface area (786 m^2 g^{-1}). The prepared PIM-1 was further modified with hydroxylamine to obtain AOPIM-1 (Figure 1a, Figure S2).[31,34] Spectroscopic characterizations of AOPIM-1 are provided in Figure S3-4, which signify the successful synthesis of the polymer. Figure 1d shows a three-dimensional view of a modeled amorphous cell of the AOPIM-1 polymer, which presents a highly microporous feature. Its specific surface area reaches 552.3 m^2 g^{-1} as deduced from its N_2 adsorption isotherm (Figure 2a). Moreover, the amidoxime modified polymer changes its solubility parameter due to the introduction of polar groups, making it soluble in common casting solvents, such as DMF, NMP, DMSO, etc (Figure S5). Unlike PIM-1 that could

only be dissolved in chloroform and tetrahydrofuran, the great solution processability of AOPIM-1 makes it feasible for the fabrication of asymmetric membranes via the industrially scalable phase inversion approach (Figure 1a). In addition, stability of AOPIM-1 under acidic and alkaline conditions are examined by immersing in acid (pH = 3) and base (pH = 10) for at least 24 h, and the chemical and physical structure of the polymer is found to remain unchanged (Figure 2a and S4). Interestingly, the AOPIM-1 polymer shows a pH-tunable chargeability (Figure 1b). Such tunable chargeability is attributed to the protonation/deprotonation of amidoxime groups, and they could thus be utilized as effective affinity sites with pH-tunability for selective adsorption and separation of oppositely charged molecules (Figure 1c). The processability, hydrophilicity, high specific surface area and pH-tunable affinity sites make AOPIM-1 a promising membrane adsorption material for aqueous-based molecular separations, which will be demonstrated in the following sections.

pH-tunable static adsorption feature of AOPIM-1 polymer

Two organic dye molecules with similar molecular weight but different charge properties, Methyl Orange (MO, MW = 327, negatively charged) and Methylene Blue (MB, MW = 320, positively charged) are used to evaluate the static adsorption behavior of AOPIM-1. As shown in Figure 2b, the amidoxime modified polymer favors the capture of negatively charged MO molecules under acidic conditions while capturing the oppositely charged MB under alkaline conditions, exhibiting a pH-tunable adsorption feature. The adsorption capacity of the polymer is found to be as high as 445.02 mg g^{-1} (MO, pH = 3.3) and 735.75 mg g^{-1} (MB, pH = 10.9), respectively, owing to the combination of high specific surface area and pH-tunable chargeability of amidoxime groups within the polymer. And lower equilibrium adsorption capacity is observed under neutral pH conditions where the amidoxime possess minimal chargeability, which also illustrates that the pH-tunable affinity sites make indispensable contribution to the adsorption capacity. As shown in Figure S7, the mixture of MB and MO is green with some precipitation due to the opposite charges of MB and MO molecules[14]. After AOPIM-1 treatment under different pH conditions, one of the colors is completely removed, and the precipitation disappears. The UV-Vis spectra clearly show the disappearance of one of the absorption peaks. The result proves that AOPIM-1 achieves the selective adsorption of MB and MO mixture by adjusting pH environment. In Figure 2c, d, Langmuir adsorption isotherms and pseudo-second-order equation ($R^2 > 0.99$) are used to fit the adsorption of AOPIM-1 on target molecules in different pH environments. Under acidic and alkaline conditions, the maximum adsorption capacity for MO and MB reaches 491.63 mg g^{-1} and 765.09 mg g^{-1}, respectively. AOPIM-1 shows a faster adsorption rate, exceeding 50% in 40 min, and reaching equilibrium in 300 min. The obtained adsorption capacity of AOPIM-1 is much higher than traditional non-porous polymer adsorbents and comparable to that of newly developed MOF adsorbents (Table S1)[18,30,36–38].

Adsorption separation of dye molecules by AOPIM-1 membranes

The adsorptive membranes based on AOPIM-1 are constructed via a wet-phase inversion method. The membrane structure is altered through tuning phase inversion conditions including various coagulation

bath composition, casting solution concentration, and casting solution composition as summarized in Table S2. With increasing ethanol content in coagulation bath, it could be observed that the structure of the membrane changes from finger-like pores (M1) to sponge-like pores (M3) as demonstrated in the cross-sectional SEM images in Figure 1e and 1f. Meanwhile, the pure water flux of resulted membrane decreases from 1505.7 L m^{-2} h^{-1} bar^{-1} (M1) to 249.8 L m^{-2} h^{-1} bar^{-1} (M3). However, the processibility capacity of M3 increases from 3.7 to 11.4 g m^{-2} which is 3 times more than that of M1 (Table S2, Figure S8-10). It should be mentioned that the effective processing capacity of membranes is calibrated under the criterion of 99% rejection ratio of Rhodamine B (RHB) (20 ppm). With increase of the concentration of the casting solution, it could be observed that the membrane thickness (M3-M5 in Table S2) is gradually increased. The increasing in thickness and processing capacity has a linear relationship from M3 11.4 g m^{-2} (64 μm) to M5 26.1 g m^{-2} (119 μm). Figure 3e and Table S3 present the comparison of AOPIM-1 membranes with reported adsorptive membranes with respect to their permeation flux and adsorptive capacity, and the dynamic adsorption capacity of the membrane appears to be 10~1000 times higher than previously reported adsorptive membranes. The above experiment results prove that by adjusting the phase inversion process, the membrane structure can be reasonably designed to achieve the purpose of rapidly removing small molecular organic pollutants in aqueous system using dynamic adsorption processes.

The dynamic adsorption separation process was conducted on a dead-end setup using a sponge-like AOPIM-1 membrane (M3). According to zeta potential measurement results, AOPIM-1 membranes exhibit positive charge at acidic pH < 4 while turning into negative charge at alkaline aqueous environment (Figure 3a). Thus, six types of organic dyes with different sizes and charges were used as target molecules for separation. Negatively charged dyes including Methyl Orange (MO), Congo Red (CR) and (BB) were tested in acidic condition and positive charged dyes including Methyl Blue (MB), RHB and Crystal Violet (CV) (Figure S11) was tested in alkaline condition. It can be seen from Figure 3b and Table S4 that under acidic conditions (pH=3), MO (99.9% rejection, 203.8 L m^{-2} h^{-1} bar^{-1}), CR (99.9% rejection, 180.9 L m^{-2} h^{-1} bar^{-1}) and BB (99.9% rejection, 192.5 L m^{-2} h^{-1} bar^{-1}) can be selectively retained. Under alkaline conditions (pH = 10), MB (99.9% rejection, 177.9 L m^{-2} h^{-1} bar^{-1}), RHB (99.9% rejection, 191.3 L m^{-2} h^{-1} bar^{-1}) and CV (99.9% rejection, 170.0 L m^{-2} h^{-1} bar^{-1}) can be retained, indicating highly efficient separation of dye molecules with different charges. The dynamic separation of two dye molecules mixture (MO/MB) is further demonstrated (Figure 3c-d). Under different pH conditions, one of the colors of the mixed solution disappears while the other color remains after filtering. The UV-Vis spectra clearly show the disappearance of one of the absorption peaks. The results prove that the AOPIM-1 membrane has the characteristic of charge selective dynamic adsorption of dye molecules. We summarized the state-of-the-art nanofiltration membranes and other membrane adsorption materials reported in the literature which are utilized for separating small organic molecules in aqueous systems (Figure 3f), and the current AOPIM-1 membranes possess 2 orders of magnitude higher flux than typical nanofiltration membranes of similar dye rejections, and surpass other reported adsorptive separation membranes in terms of water flux and dye rejection.

The adsorptive separation behavior of the AOPIM-1 membrane is further demonstrated in a multi-cycle dynamic membrane adsorption process. It can be seen from Figure 4a that the flux of the membrane decreases with the increasing permeation volume in each cycle, which can be attributed to the accumulation of dyes on the surface and inside of the adsorptive membrane. In the first seven cycles, 20-30 mL of methanol was adopted as a feed solution to desorb the dye molecules from the membrane for a short time (within 5 minutes). It can be seen in digital photo in Figure 4d that the color of the membrane due to the adsorption of dye disappears after cleaning. At the same time, the flux recovery rate (FRR) in each cycle reaches 98%. After 7 cycles, a long-term desorption treatment (about 2 hours by methanol) on the membrane was performed, and a higher recovery rate is got. The Brunauer-Emmet-Teller (BET) surface area of the AOPIM-1 adsorptive membrane is reduced from 552.3 $m^2 g^{-1}$ to 415.4 $m^2 g^{-1}$ after the adsorption test, and it can be easily regenerated to the original level after desorption (Figure 4b). Meanwhile, it can be seen in Figure 4c, the pore size distribution of AOPIM-1 is also restored to the original level after cleaning. As a control group, a negatively charged polyethersulfone ultrafiltration membrane prepare by phase inversion was selected to test positively charged organic small molecules. It is found that almost all dye molecules pass through the membrane without noticeable retention (Figure S12), which is common for conventional ultrafiltration membranes that rejects large molecules and particulate matter (such as proteins, suspended solids, bacteria, viruses, and colloids) but cannot accurately separate small organic molecules[10]. Without necessary specific surface area and affinity sites for effective adsorption, membranes of conventional polymer materials require further reduced the pore size for separation of small molecules, but it will inevitably lead to a significant reduction in water flux and huge energy consumption. The above results reveal that the electrostatic attraction, micropore and membrane pore structure co-govern the dynamic adsorption performance of the membrane.

Adsorptive separation of active pharmaceutical ingredients (APIs)

In the pharmaceutical industry, precise separation of organic molecules such as drugs, proteins, and polysaccharides are indispensable for the production of active pharmaceutical ingredients (APIs)[5,7,56]. For instance, the raw material water extracts of phytochemical drugs, an important category of APIs extracted from natural plants[45], usually possess a complex composition including polysaccharides (molecular weights usually range from 10,000 to 100, 000 Da), APIs (molecular weight < 2000 Da), and inorganic salts such as sodium chloride. The feasibility of membrane adsorption for the separation of such 3-component systems was evaluated in this section. As schematically illustrated in Figure 5a and Figure S13, a 2-step process is proposed for adsorptive separation of a phytochemical drug water extract using AOPIM-1 membranes. In the first step, the water extract of natural plants passes through the surface of the membrane, the plant polysaccharides with large molecular weight are trapped on the feed side of the membrane, the active pharmaceutical molecules with small molecular weight are adsorbed within the membrane matrix, and inorganic salts are permeated through the membrane. After the

membrane is saturated with API adsorption, the second step uses methanol as the eluent to flow in from the feed side, and the API eluate is obtained on the permeate side.

As a proof of concept, an AOPIM-1 membrane with altered casting conditions (3:1 DMF/1,4-dioxane co-solvent[47−48]) and tightened membrane pores (water flux of ~121.3 L m^{-2} h^{-1} bar^{-1}, MWCO of ~20 kDa) are prepared, and the MWCO curve of M6 and the pore size distribution are shown in Figure S14. A synthetic water extract (Table S5) is prepared with Dextran T-200 (MW = 20 kDa) used as the target macromolecular polysaccharide, berberine (MW = 336.4 Da) as the target small API molecule, and sodium chloride as the inorganic salt. As can be seen in Figure 5b, during a cross-flow filtration cycle, berberine is continuously adsorbed in the membrane, and the rejection rate of Dextran T-200 is maintained above 90%. At the same time, sodium chloride permeates through the membrane without rejection. At the end of one filtration cycle, the feed solution is changed to methanol to elute the berberine enriched in the membrane. Figure S15 clearly shows the UV-Vis absorption peaks in the stock solution and filtrate before and after processing 50 mL of the synthetic feed. After the filtration, the characteristic absorption peak of berberine disappeared, which proves that the berberine in the feed solution are completely adsorbed in the membrane. At the same time, it can be seen in the illustration that 50 mL of the feed solution is enriched in the membrane and finally eluted by about 5 mL of methanol, achieving a 10-fold enrichment. Compared with other separation methods, the traditional distillation method is energy-intensive and time-consuming, whereas the membrane filtration method is difficult to achieve sufficient accuracy and efficiency, and the obtained permeate usually requires further purification operations afterwards[57]. The membrane adsorption separation method shows the merit of smallest energy consumption and highest product purity. More importantly, this experiment demonstrates that the ultrahigh processing capacity of AOPIM-1 adsorptive membranes omits the need of frequent cleaning and regeneration, effectively broaden the application feasibility of membrane adsorption from treating trace organic compounds towards mass chemical productions.

Conclusions

This work has developed a new type of pH-tunable high-capacity adsorptive membranes based on AOPIM-1, in which the high specific surface area (high adsorption capacity), abundant adsorption sites (adsorption selectivity), reversible adsorbate-adsorbent interaction (fast adsorption/desorption rates), good solubility processability (scale-up feasibility) and hydrophilicity (easy-wet micropores) of AOPIM-1 are fully utilized. The processing capacity and permeability of the membrane is adjusted by manipulating the phase inversion process. While achieving the retention of small molecules, the membrane permeation flux is in line with the level of common ultrafiltration, which is 2 orders of magnitude higher than typical nanofiltration membranes of similar rejections. The best processing capacity reaches 26.114 g m^{-2}, which is 10~1000 times higher than the value reported in the literature for existing adsorptive membranes. This newly developed membrane material realizes a dynamic operation process of membrane adsorption-desorption, cleaning, and regeneration with high efficiency, which can be a good supplement to conventional pressure-driven membrane separation processes. Owing to the

unprecedented adsorption capacity, the AOPIM-1 membrane exhibits high separation efficiency of actual complex systems and highly guarantees the purity of the product obtained. The development of AOPIM-1 adsorptive membranes thereby broadens the prospects of membrane adsorption for practical applications.

Methods

Fabrication of PIM-1 and AOPIM-1 polymers. Polymer of intrinsic microporosity (PIM-1) was obtained following a previously reported method. Under a nitrogen atmosphere, 3.001 g (15 mmol) tetra-fluoroterephthalonitrile (TFTPN), 5.106 g (15 mmol) 5,5',6,6'-tetrahydroxy-3,3,3',3'-tetramethylspirobisindane (TTSBI) and 30 mL anhydrous DMAc were added into a 100 mL three-necked flask. After the chemicals were completely dissolved, 6.21 g (45 mmol) anhydrous milled K_2CO_3 was added and the flask was placed into an 160°C oil bath under mechanical stirring. After approximately 3 min, a viscous yellow solution formed, and 20 mL of toluene was added. Several minutes later, a further 20 mL of toluene was added to dilute the solution. Then, the mixture was poured into 300 mL methanol, and an elastic, threadlike, light yellow polymer was observed. The polymer product was dissolved in chloroform and reprecipitated in methanol, and then refluxed in Milli-Q water for 4-5 h and dried at 80°C under vacuum for 48 h.

Hydrophilic amidoxime modified PIM-1 (AOPIM-1) was synthesized by dissolving 0.5 g PIM-1 in 30 mL THF and heating to reflux under N_2. Then, 5.0 mL hydroxyl amine was added dropwise, and the solution was further refluxed for 20 hours. The resulting polymer was precipitated by the addition of ethanol, filtered, washed thoroughly with ethanol and water, and then dried at 110°C for 24 h.

Fabrication of AOPIM-1 membranes. The polymer dope was obtained by dissolving AOPIM-1 in DMF or DMF/1,4-dioxane mixed solvent, and stirred continuously at room temperature overnight to ensure that the polymer dissolves evenly in the solvent. Then the mixture was left at room temperature for 24 h to remove air bubbles. After that, the polymer solution was used to cast films on a clean glass plate at 25 ºC and 40% relative humidity. For the casting solution with co-solvent, the solvent was allowed to evaporate from the surface of the film in 20 s to produce a denser selective skin. Next, the glass plate was immersed into a coagulation bath. After 1 h, membranes were transferred to a fresh water bath and kept for 24 h to finish phase separation. Finally, the membranes were immersed in methanol for future use.

Membrane material characterization. The morphology of the as-prepared membranes was observed using a field emission scanning electron microscope (Hitachi S4800, Japan). Before capturing SEM image, a thin Au layer was sputtered onto the membrane under 10 mA for 2 min (Emitech K550X sputtering). ^{1}H nuclear magnetic resonance (NMR) spectra were recorded on a Bruker 400 MHz spectrometer using dimethyl sulfoxide-d_6 as a solvent. FTIR spectra of membranes were obtained using a Nicolet 6700 FTIR spectrometer (USA). Nitrogen absorption/desorption measurements were performed on a Quantachrome Autosorb IQ-MP-MP at 77 K. All samples were degassed at 120°C for 12 h before nitrogen absorption measurements were performed. The surface charge of the membrane was

determined by streaming potential measurement using a SurPASS 3 electrokinetic analyzer with a flat-plate measuring cell (10 mm × 20 mm).

Static adsorption behavior of AOPIM-1 polymer. The static adsorption behavior of AOPIM-1 was investigated using dyes with different chargeability (negative, MO; positive, MB) as model solutes. A dry AOPIM-1 membrane coupon (~10 mg) was placed in dye solution with certain concentration (10-500 mg L^{-1}) and pH value. The mixture was stirred continuously at room temperature at least 24 h or a certain time. The concentration of dyes was analyzed by a UV-Vis spectrophotometer (PerkinElmer, Inc.). The amount of dye adsorbed by the AOPIM-1, q (mg g^{-1}), was determined from the Eq. (1)[49–50],

$$q = \frac{\left(C_0 - C_*\right)\mathrm{V}}{\mathrm{w}} \quad (1)$$

where q represents the adsorption amount at equilibrium (q_e) or the adsorption amount at time t (q_t). C_0 (mg L^{-1}), C_* (mg L^{-1}), V (L), and W (g) represent initial concentration of dye, concentration of dye at equilibrium or time t, volume of solution and amount of AOPIM-1, respectively.

The effect of pH on the adsorption was studied by adjusting pH of the dye solutions to 3-10 with the help of 0.1 M NaOH and 0.1 M HCl.

The adsorption kinetics of dyes by AOPIM-1 was studied using a second-order equation in nonlinear form by Ep. (2)[54–55],

$$q_t = \frac{k_2 q_e^2 t}{1 + k_2 q_e t} \quad (2)$$

where k_2 (g mg^{-1} min^{-1}) is the second-order rate constant. The adsorption capacity of dyes by AOPIM-1 was studied using a Langmuir isotherm model by Ep. (3)[54–55],

$$q_e = \frac{K_L q_m C_e}{1 + K_L C_e} \quad (3)$$

where K_L (L mg^{-1}) represents the affinity constant and q_m (mg g^{-1}) is the maximum adsorption capacity of the adsorbate.

Dynamic adsorptive separation properties of AOPIM-1 membranes The dynamic adsorption properties of AOPIM-1 membranes were investigated using six types of dyes with different chargeability (negative: MO, CR, BB; positive: MB, RHB, CV). Filtration experiments were performed in a dead-end filtration cell with an effective membrane area of 3.14 cm^2 (Figure S16). Each tested membrane was compacted by the filtration of deionized water under 0.2 MPa for 2 h in order to achieve a steady flux. Then, the permeate flux (J (L m^{-2} h^{-1} bar^{-1})) used different dyes as feed solution (20 mg L^{-1}, PH=3/10) was measured under 0.2 MPa at room temperature and calculated using the following Eq. (4),

$$J = \frac{V}{\Delta PAt} \quad (4)$$

where ΔP (bar), V (L), A (m^2), and t (h) represent permeate flux, transmembrane pressure, permeate volume, membrane area and filtration time, respectively. The rejection rate (R (%)) of dyes was calculated from Eq. (5),

$$R = 1 - \frac{C_P}{C_F} \quad (5)$$

where C_P and C_F correspond to the dye concentrations in the permeate and feed solutions, respectively. The dye concentrations in the permeate and feed solutions were determined using a UV/Vis spectrometer (Biochrom Libra S32). The processing capacity used RHB as feed solution (20 mg L^{-1}, PH=10) was measured under 0.2 MPa at room temperature and determined by permeation volume when rejection is higher than 99%.

The multi-cycle adsorptive separation performance stability of the AOPIM-1 adsorptive membrane was performed in a dead-end filtration cell with an effective membrane area of 3.14 cm^2 for 8 cycles. For a typical cycle, the RHB solution (20 mg L^{-1}, pH = 10) was filtrated through the membrane for 500 L m^{-2} at 0.2 MPa, and the permeate flux (J) was calculated by Eq. (4). Afterwards, the membrane is subjected to a short time (five minutes) desorption process by switching the feed solution of the membrane to about 20 ml methanol for cleaning, and the eluent can be obtained at the outlet. After that, fresh feed dye solution was applied for the next cycle.

Adsorptive separation of APIs by AOPIM-1 membranes Separation of a synthetic 3-conponent mixture feed representing inorganic salt, polysaccharides and active pharmaceutical ingredient (API) chemicals in the water extract of natural plants was performed in a lab-scale cross-flow cell (Figure S13) at room temperature. The feed solution included NaCl, dextran T-200 and berberine with detailed composition listed in Table S5. The concentrations of each substance in the feed and permeate solution were measured by conductometer (FE30K, Mettler Toledo), total organic carbon (TOC) analyzer (Aurora 1030W) and UV-Vis spectrophotometer (PerkinElmer, Inc.), respectively.

Declarations

Acknowledgements

This work was supported by the National Key R&D Program of China (2019YFC1711300, 2019YFA0705800), the National Natural Science Funds for Distinguished Young Scholar (51625306), the National Natural Science Foundation of China (21988102, 51803145, 51873230), Funding supports from the Social Development Program of Jiangsu Province (BE2019678) and Chinese Academy of Sciences are gratefully appreciated as well.

Author contributions

Z. W., W. F., and J. J. conceived the initial idea and experimental design. L. X. performed the membrane fabrication and characterization experiments. W. F. and J. J. supervised the study and experiments. K. L. carried out the molecular dynamics simulations and analysed the data. All authors analysed results and commented on the manuscript. Z. W., L. X., W. F. and J. J. co-wrote the paper with help from all authors.

Additional information

Supplementary information is available for this paper on line.

Correspondence and requests for materials should be addressed to W. F. or J. J.

References

1. Sholl, D. S. & Lively, R. P. Seven chemical separations to change the world. *Nature* **532**, 435–437 (2016).
2. Shannon, M. A., Bohn, P. W., Elimelech, M., Georgiadis, J. G., Marinas, B. J. & Mayes, A. M. Science and technology for water purification in the coming decades. *Nature* **452**, 301–310 (2008).
3. Pintor, A. M. A., Vilar, V. J. P., Botelho, C. M. S. & Boaventura, R. A. R. Oil and grease removal from wastewaters: Sorption treatment as an alternative to state-of-the-art technologies. A critical review. *Chem. Eng. J.* **297**, 229–255 (2016).
4. Buonomenna, M. G. & Bae, J. Organic Solvent Nanofiltration in Pharmaceutical Industry. *Sep. Purif. Rev.* **44**, 157–182 (2015).
5. Abels, C., Carstensen, F. & Wessling, M. Membrane processes in biorefinery applications. *J. Membrane. Sci.* **444**, 285–317 (2013).
6. Marchetti, P., Jimenez Solomon, M. F., Szekely, G. & Livingston, A. G. Molecular separation with organic solvent nanofiltration: a critical review. *Chem. Rev.* **114**, 10735–10806 (2014).
7. Park, H. B., Kamcev, J., Robeson, L. M., Elimelech, M. & Freeman, B. D. Maximizing the right stuff: The trade-off between membrane permeability and selectivity. *Science* **356**, 1138–1148 (2017).
8. Wang, Z., Wang, Z., Lin, S., Jin, H., Gao, S., Zhu, Y. & Jin, J. Nanoparticle-templated nanofiltration membranes for ultrahigh performance desalination. *Nat. Commun.* **9**, 2004 (2018).
9. Fane, A. G., Wang, R. & Hu, M. X. Synthetic membranes for water purification: status and future. *Angew. Chem. Int. Ed.* **54**, 3368–3386 (2015).
10. Bellona, C., Drewes, J. E., Xu, P. & Amy, G. Factors affecting the rejection of organic solutes during NF/RO treatment--a literature review. *Water. Res.* **38**, 2795–2809 (2004).
11. Alsbaiee, A., Smith, B. J., Xiao, L., Ling, Y., Helbling, D. E. & Dichtel, W. R. Rapid removal of organic micropollutants from water by a porous beta-cyclodextrin polymer. *Nature* **529**, 190–194 (2016).
12. Satilmis, B., Isık, T., Demir, M. M. & Uyar, T. Amidoxime functionalized Polymers of Intrinsic Microporosity (PIM-1) electrospun ultrafine fibers for rapid removal of uranyl ions from water. *Appl. Surf. Sci.* **467-468**, 648–657 (2019).

13. Wang, Z., Cui, F., Pan, Y., Hou, L., Zhang, B., Li, Y. & Zhu, L. Hierarchically micro-mesoporous beta-cyclodextrin polymers used for ultrafast removal of micropollutants from water. *Carbohyd. Polym.* **213**, 352–360 (2019).
14. Dong, Z., Wang, D., Liu, X., Pei, X., Chen, L. & Jin, J. Bio-inspired surface-functionalization of graphene oxide for the adsorption of organic dyes and heavy metal ions with a superhigh capacity. *J. Mater. Chem. A.* **2**, 5034–5040 (2014).
15. Boi, C., Dimartino, S. & Sarti, G. C. Modelling and simulation of affinity membrane adsorption. *J. Chromatogr. A.* **1162**, 24–33 (2007).
16. Ghosh, R. Protein separation using membrane chromatography: opportunities and challenges. *J. Chromatogr. A.* **952**, 13–27 (2002).
17. Uliana, A. A., Bui, N. T., Kamcev, J., Taylor, M. K., Urban, J. J. & Long, J. R. Ion-capture electrodialysis using multifunctional adsorptive membranes. *Science* **372**, 296–299 (2021).
18. Wang, H., Zhao, S., Liu, Y., Yao, R., Wang, X., Cao, Y., Ma, D., Zou, M., Cao, A., Feng, X. & Wang, B. Membrane adsorbers with ultrahigh metal-organic framework loading for high flux separations. *Nat. Commun.* **10**, 4204 (2019).
19. Fenton, J. L., Burke, D. W., Qian, D., Cruz, M. O. & Dichtel, W. R. Polycrystalline Covalent Organic Framework Films Act as Adsorbents, Not Membranes. *J. Am. Chem. Soc.* **143**, 1466–1473 (2021).
20. Hao, S., Jia, Z., Wen, J., Li, S., Peng, W., Huang, R. & Xu, X. Progress in adsorptive membranes for separation-A review. *Sep. Purif. Technol.* **255**, 117772 (2021).
21. Ting, H., Chi, H.-Y., Lam, C. H., Chan, K.-Y. & Kang, D.-Y. High-permeance metal–organic framework-based membrane adsorber for the removal of dye molecules in aqueous phase. *Environ. Sci-Nano.* **4**, 2205–2214 (2017).
22. Zong, L., Yang, Y., Yang, H. & Wu, X. Shapeable Aerogels of Metal-Organic-Frameworks Supported by Aramid Nanofibrils for Efficient Adsorption and Interception. *ACS Appl. Mater. Inter.* **12**, 7295–7301 (2020).
23. Wang, Z., Zhang, B., Fang, C., Liu, Z., Fang, J. & Zhu, L. Macroporous membranes doped with micro-mesoporous beta-cyclodextrin polymers for ultrafast removal of organic micropollutants from water. *Carbohyd. Polym.* **222**, 114970 (2019).
24. Wang, Z., Guo, S., Zhang, B., Fang, J. & Zhu, L. Interfacially crosslinked beta-cyclodextrin polymer composite porous membranes for fast removal of organic micropollutants from water by flow-through adsorption. *J. Hazard. Mater.* **384**, 121187 (2020).
25. Liang, H. W., Cao, X., Zhang, W. J., Lin, H. T., Zhou, F., Chen, L. F. & Yu, S. H. Robust and Highly Efficient Free-Standing Carbonaceous Nanofiber Membranes for Water Purification. *Adv. Funct. Mater.* **21**, 3851–3858 (2011).
26. Furukawa, H., Cordova, K. E., O'Keeffe, M. & Yaghi, O. M. The chemistry and applications of metal-organic frameworks. *Science* **341**, 1230444 (2013).
27. McKeown, N. B. & Budd, P. M. Polymers of intrinsic microporosity (PIMs): organic materials for membrane separations, heterogeneous catalysis and hydrogen storage. *Chem. Soc. Rev.* **35**, 675–

683 (2006).

28. Wang, Z., Wang, D., Zhang, S., Hu, L. & Jin, J. Interfacial Design of Mixed Matrix Membranes for Improved Gas Separation Performance. *Adv. Mater.* **28**, 3399–3405 (2016).
29. Wang, Z., Wang, D. & Jin, J. Microporous Polyimides with Rationally Designed Chain Structure Achieving High Performance for Gas Separation. *Macromolecules* **47**, 7477–7483 (2014).
30. Zhang, C., Pei, L., Huang, W. & Bing, C. Selective adsorption and separation of organic dyes in aqueous solutions by hydrolyzed PIM-1 microfibers. *Chem. Eng. Res. Des.* **109**, 76–85 (2016).
31. Patel, H. A. & Yavuz, C. T. Noninvasive functionalization of polymers of intrinsic microporosity for enhanced CO_2 capture. *Chem. Commun.* **48**, 9989–9991 (2012).
32. Tan, R., Wang, A., Malpass-Evans, R., Williams, R., Zhao, E. W., Liu, T., Ye, C., Zhou, X., Darwich, B. P., Fan, Z., Turcani, L., Jackson, E., Chen, L., Chong, S. Y., Li, T., Jelfs, K. E., Cooper, A. I., Brandon, N. P., Grey, C. P., McKeown, N. B. & Song, Q. Hydrophilic microporous membranes for selective ion separation and flow-battery energy storage. *Nat. Mater.* **19**, 195–202 (2020).
33. Luo, X., Wang, Z., Wu, S., Fang, W. & Jin, J. Metal ion cross-linked nanoporous polymeric membranes with improved organic solvent resistance for molecular separation. *J. Membrane. Sci.* **621**, 119002 (2021).
34. Wang, Z., Ren, H., Zhang, S., Zhang, F. & Jin, J. Polymers of intrinsic microporosity/metal-organic framework hybrid membranes with improved interfacial interaction for high-performance CO_2 separation. *J. Mater. Chem. A.* **5**, 10968–10977 (2017).
35. Wang, Z. G., Liu, X., Wang, D. & Jin, J. Tröger's base-based copolymers with intrinsic microporosity for CO_2 separation and effect of Tröger's base on separation performance. *Polym. Chem.* **5**, 2793–2800 (2014).
36. Liu, L., Ma, Y., Yang, W., Chen, C., Li, M., Lin, D. & Pan, Q. Reusable ZIF-8@chitosan sponge for the efficient and selective removal of congo red. *New. J. Chem.* **44**, 15459–15466 (2020).
37. Satilmis, B. & Budd, P. M. Selective dye adsorption by chemically-modified and thermally-treated polymers of intrinsic microporosity. *J. Colloid. Interf. Sci.* **492**, 81–91 (2017).
38. Jing, R., Yan, C., Liu, Q., Yang, Q. & Li, Y. Preparation of amidoxime-modified polyacrylonitrile nanofibrous adsorbents for the extraction of copper(II) and lead(II) ions and dye from aqueous media. *J. Appl. Polym. Sci.* **135**, 45697 (2017).
39. Zhao, S., & Wang, Z. A loose nano-filtration membrane prepared by coating HPAN UF membrane with modified PEI for dye reuse and desalination. *J. Membrane. Sci.*, **524**, 214–224 (2017).
40. Lin, J., Ye, W., Zeng, H., Yang, H., Shen, J., Darvishmanesh, S., & Van der Bruggen, B. Fractionation of direct dyes and salts in aqueous solution using loose nanofiltration membranes. *J. Membrane. Sci.*, **477**, 183–193 (2015).
41. Yang, Z., Zhou, Z. W., Guo, H., Yao, Z., Ma, X. H., Song, X., & Tang, C. Y. Tannic acid/Fe^{3+} nanoscaffold for interfacial polymerization: toward enhanced nanofiltration performance. *Environ. Sci. Technol.*, **52**, 9341–9349 (2018).

42. Yu, L., Zhang, Y., Zhang, H., & Liu, J. Development of a molecular separation membrane for efficient separation of low-molecular-weight organics and salts. *Desalination*, **359**, 176–185 (2015).
43. You, F., Xu, Y., Yang, X., Zhang, Y. & Shao, L. Bio-inspired Ni (2+)-polyphenol hydrophilic network to achieve unconventional high-flux nanofiltration membranes for environmental remediation. *Chem. Commun.* **53**, 6128–6131 (2017).
44. Hu, M., & Mi, B. Enabling graphene oxide nanosheets as water separation membranes. *Environ. Sci. Technol.*, **47**, 3715–3723 (2013).
45. Zhao, R., Ma, T., Cui, F., Tian, Y. & Zhu, G. Porous Aromatic Framework with Tailored Binding Sites and Pore Sizes as a High-Performance Hemoperfusion Adsorbent for Bilirubin Removal. *Adv. Sci.* **7**, 2001899 (2020).
46. Tan, L., Gong, L., Wang, S., Zhu, Y., Zhang, F., Zhang, Y. & Jin, J. Superhydrophilic Sub-1-nm Porous Membrane with Electroneutral Surface for Nonselective Transport of Small Organic Molecules. *ACS Appl. Mater. Inter.* **12**, 38778–38787 (2020).
47. Soroko, I., Lopes, M. P. & Livingston, A. The effect of membrane formation parameters on performance of polyimide membranes for organic solvent nanofiltration (OSN): Part A. Effect of polymer/solvent/non-solvent system choice. *J. Membrane. Sci.* **381**, 152–162 (2011).
48. See-Toh, Y. H., Silva, M. & Livingston, A. Controlling molecular weight cut-off curves for highly solvent stable organic solvent nanofiltration (OSN) membranes. *J. Membrane. Sci.* **324**, 220–232 (2008).
49. Xing, T., Kai, H. & Chen, G. Study of adsorption and desorption performance of acid dyes on anion exchange membrane. *Color. Technol.* **128**, 295–299 (2012).
50. Yuan, L. Y., Gao, G., Feng, C. Q., Chai, Z. F. & Shi, W. Q. A new family of actinide sorbents with more open porous structure: Fibrous functionalized silica microspheres. *Chem. Eng. J.* **385**, 123892 (2020).

Figures

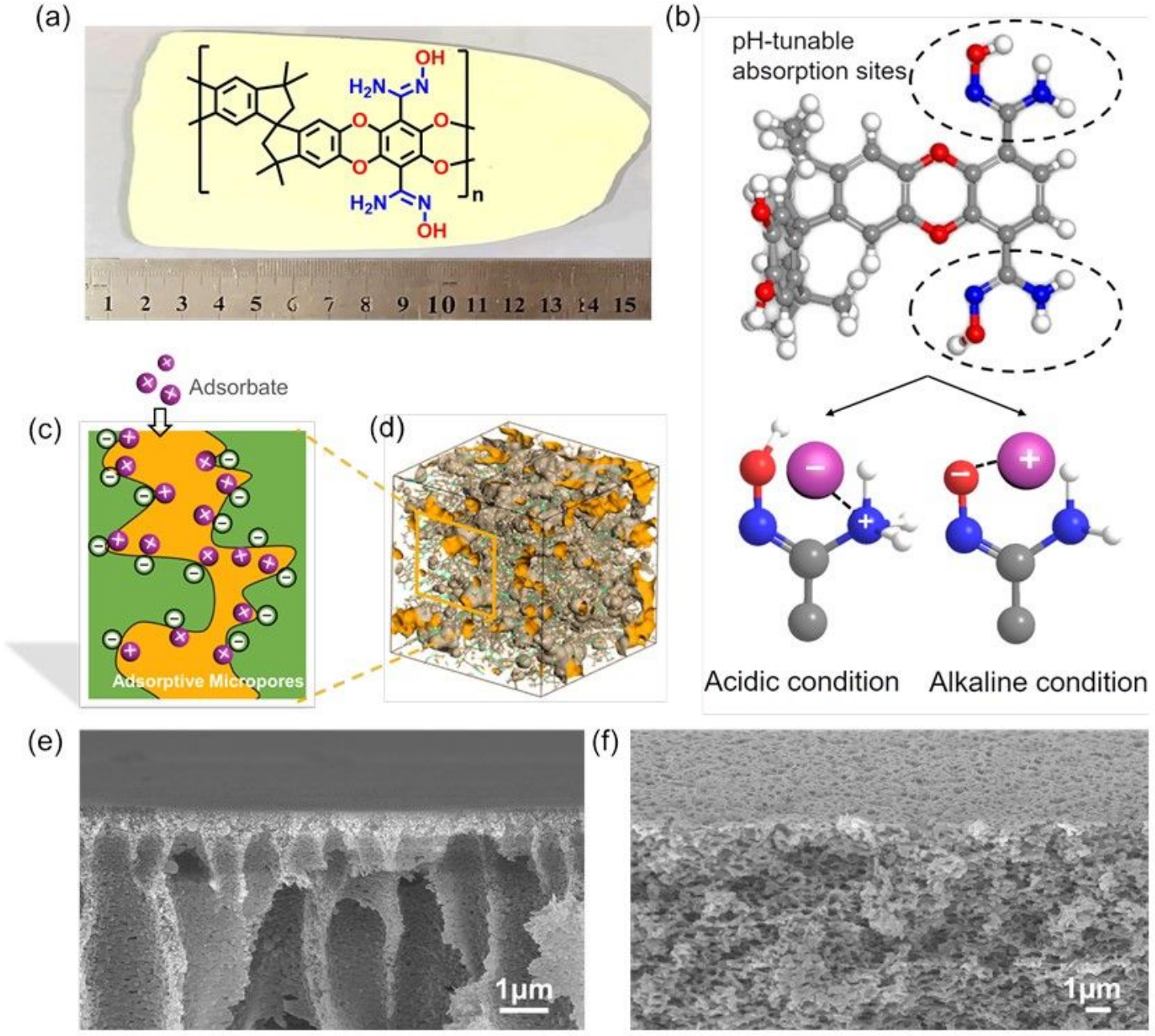

Figure 1

(a) Chemical structure of AOPIM-1 polymer and optical image of AOPIM-1 membrane; (b) The pH-tunable chargeability of AOPIM-1 under acidic or alkaline conditions, where the gray, white and red spheres represent C atoms, H atoms and O atoms, respectively; (c) Schematic diagram of microporous polymer membranes for adsorptive separation of organic molecules; (d) Three-dimensional view of an amorphous cell of the AOPIM-1 polymer. The brown surface indicates the van der Waals surface, and the orange surface is the Connolly surface with a probe radius of 1.6 Å; Cross-section SEM images of the AOPIM-1 membranes obtained by phase conversion of different coagulation bath compositions: (e) H2O:EtOH = 100:0 and (f) H2O:EtOH = 0:100.

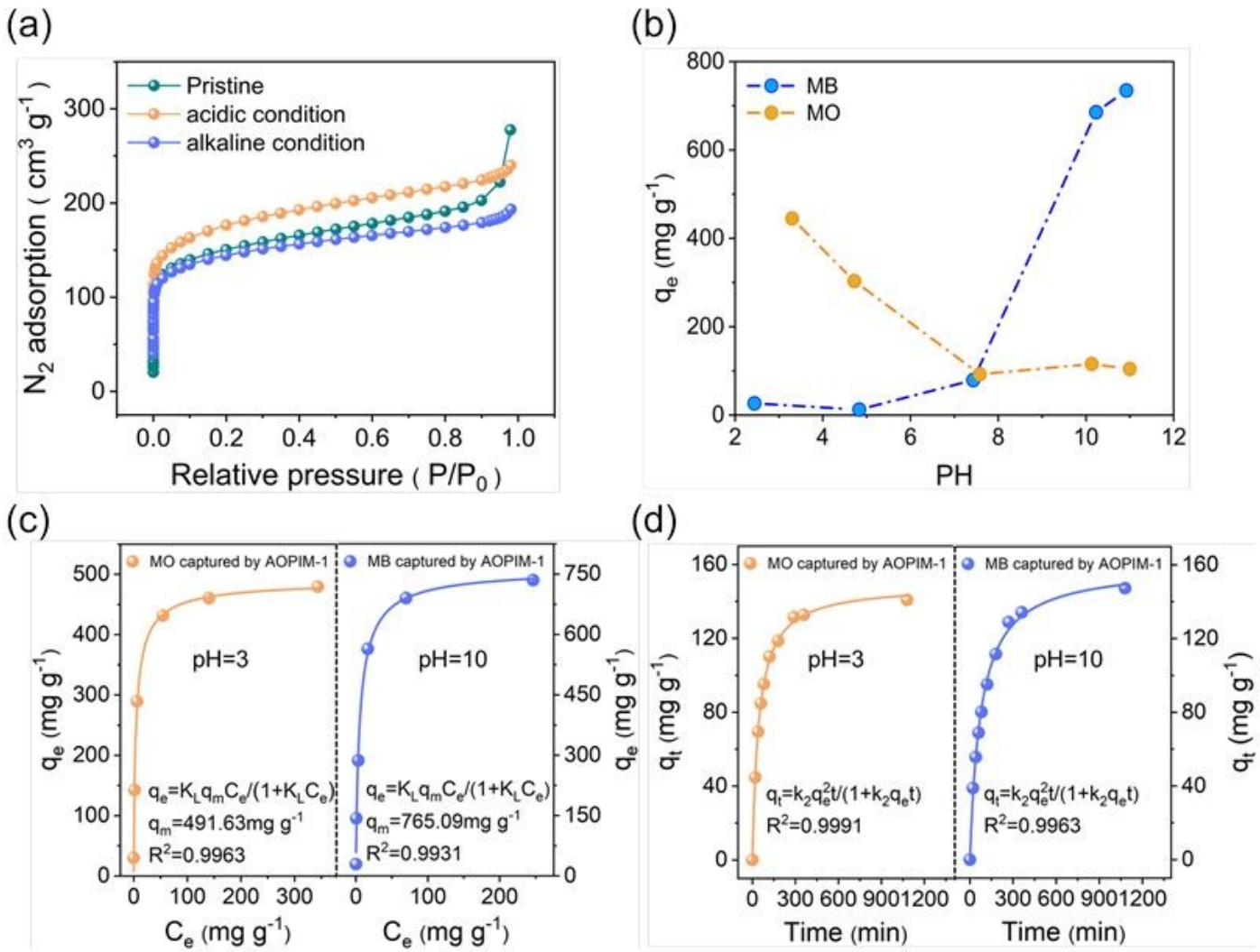

Figure 2

pH-tunable static adsorption feature of AOPIM-1 polymer. (a) Nitrogen absorption isotherms of AOPIM-1 as-prepared and after immersing in acid (pH=3) or base (pH=10) for at least 24 h; (b) Equilibrium adsorption capacity (qe) of AOPIM-1 for MO and MB dye molecules at different pH conditions; (c) Adsorption isotherm of MO and MB by AOPIM-1 at acidic and alkaline conditions, respectively (qe: equilibrium adsorption capacity, qm: maximum adsorption capacity, Ce: concentration of dye molecules at equilibrium); (d) Adsorption of MO and MB by AOPIM-1 as a function of contact time at acidic and alkaline conditions, respectively (qt: adsorption amount at time t).

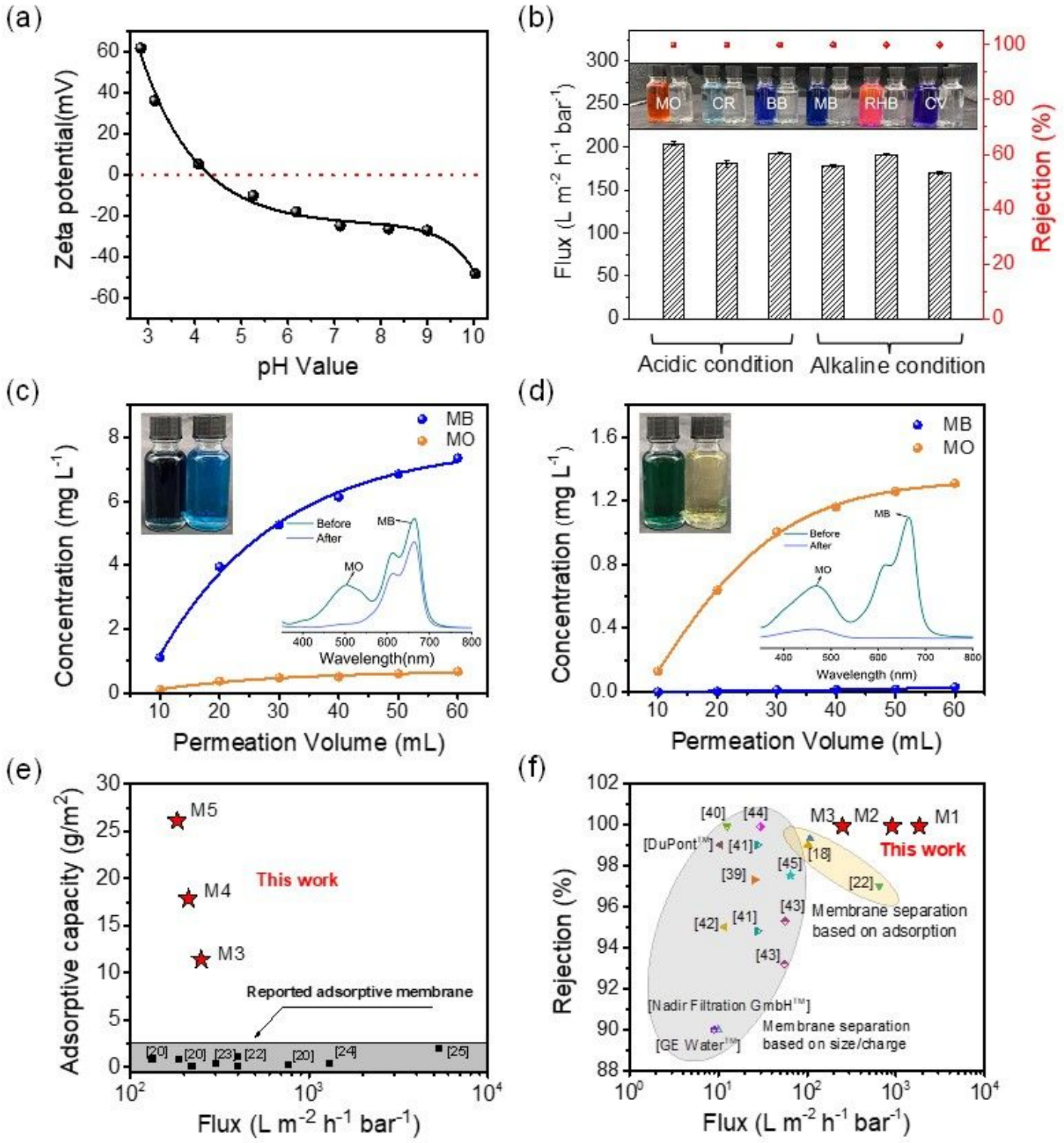

Figure 3

Charge-selective dynamic adsorption of organic dye molecules by AOPIM-1 membranes. (a) Zeta potential of AOPIM-1 membrane at pH 3-10; (b) The dynamic separation performance of AOPIM-1 membrane at different pH condition for different dyes (concentration 20 ppm, applied pressure 0.2 MPa, pH = 3/10); (c, d) The separation (MO/MB) of two dye molecules with similar molecular weights but different charges under different pH condition (concentration 10 ppm MO + 10 ppm MB, applied pressure

0.2 MPa, pH = 3/10); (e) Comparison of AOPIM-1 membranes with reported adsorptive membranes with respect to their permeation flux and adsorptive capacity; (f) Comparison of AOPIM-1 membranes with reported membranes with respect to their permeation flux and dye rejection/removal efficiency.

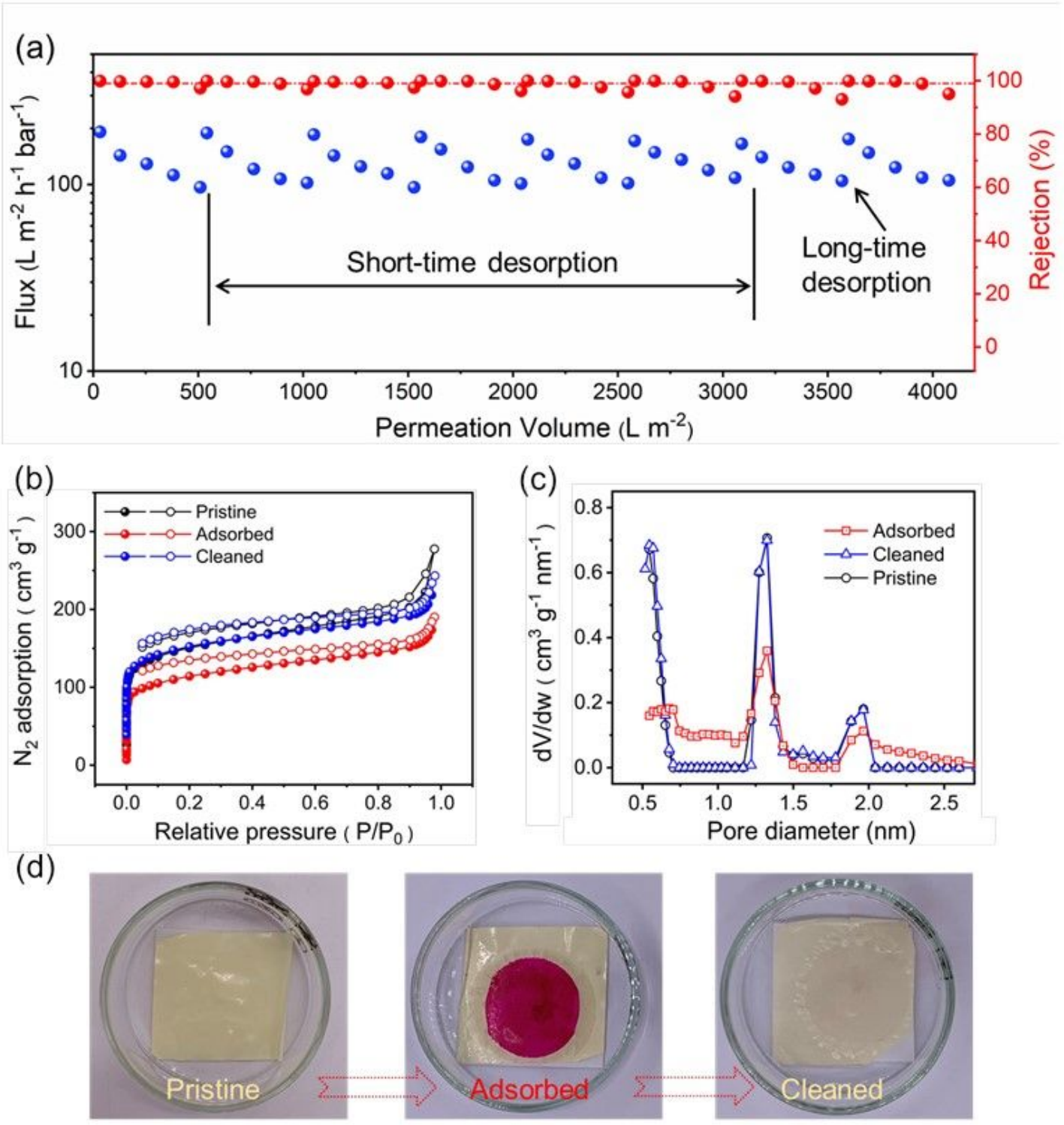

Figure 4

Adsorptive separation behavior of AOPIM-1 membrane in a multi-cycle dynamic adsorption-desorption process. (a) Flux and RHB removal rate of the membrane in multiple adsorption-desorption cycles

(concentration: 20 ppm, applied pressure: 0.2 MPa, pH = 10); (b) Pore size distributions of pristine, adsorbed and desorbed AOPIM-1 membrane, respectively; (c) Nitrogen absorption-desorption isotherms of pristine, adsorbed and desorbed AOPIM-1, respectively; (d) optical pictures of the pristine, adsorbed and cleaned AOPIM-1 membrane coupon.

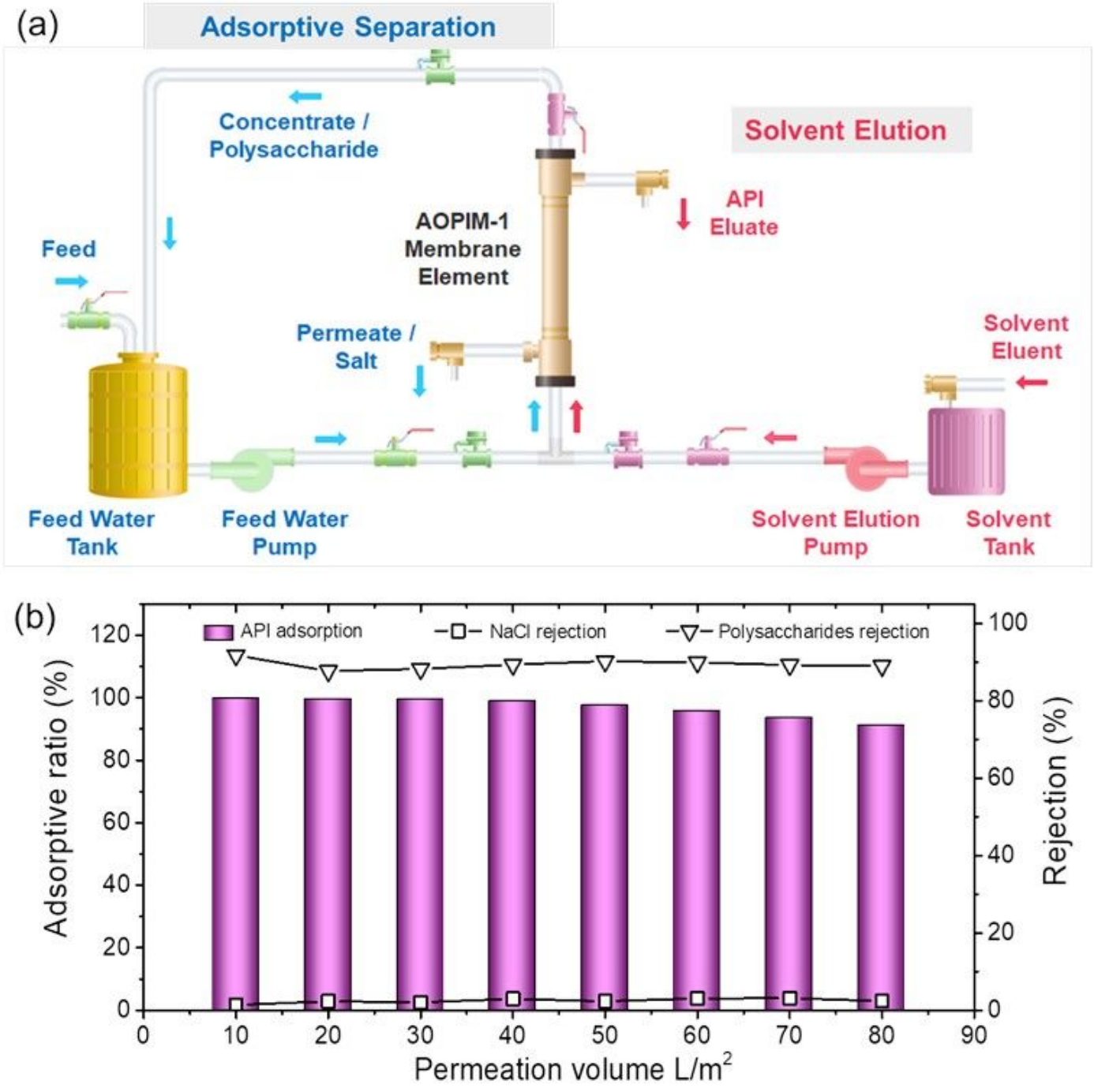

Figure 5

Adsorptive separation of active pharmaceutical ingredients (APIs) by AOPIM-1 membranes. (a) Schematic illustration of the 2-step process for adsorptive separation of mixed API/polysaccharide/salt

feed using AOPIM-1 membranes; (b) The adsorption/rejection ratio of API/polysaccharide/NaCl versus permeation volume of a synthetic water extract feed solution.

Supplementary Files

This is a list of supplementary files associated with this preprint. Click to download.

- Supportinginformation.docx